small NANO MICRO

Molecular dynamics

Tunable Water Channels with Carbon Nanoscrolls

*Xinghua Shi, Yuan Cheng, Nicola M. Pugno, and Huajian Gao**

***M**olecular dynamics simulations and theoretical analyses are performed to show that the flow rate of water through the core of carbon nanoscrolls (CNSs) can be adjusted over a broad range through the effective surface energy, which in turn can be tuned by an applied DC or AC electric field. The results suggest that the CNSs hold great promise for applications such as tunable water and ion channels, nanofluidic devices, and nanofilters, as well as tunable gene- and drug-delivery systems.*

Keywords:
- graphene
- ion channels
- molecular dynamics
- nanostructures
- water channels

1. Introduction

Water transport through channel proteins across cell membranes has long been of strong interest to cell biology.[1–3] The development of nanotechnology has expanded the scope of water channels to including nanomaterials such as carbon nanotubes (CNTs). It has been shown that a single-walled CNT (SWCNT) can host a single chain of water molecules that can burst out of the CNT spontaneously.[4] This study has inspired a series of further studies on tunable CNT-based water channels. So far, a number of approaches have been explored in the literature to control water transport through a CNT, including use of an external force to adjust the internal capacity of the CNT[5] and application of an electric field to change the dipole orientations of the confined water chain,[6,7] as well as ways to polarize carbon atoms[8–10] and to change electrostatic interactions by adding ions[11,12] in the system.

Due to their rigid, closed tubular structure, the CNT-based water channels only have limited permeability. Here we propose a class of novel, tunable water channels based on carbon nanoscrolls (CNSs) whose core radius can be tuned over a broad size range by an applied DC/AC electric field. CNSs consist of a continuous graphene sheet rolled up in a spiral form. In contrast to the closed tubular structure of CNTs, the spiral structure of CNSs is much more flexible in the radial direction and thus more sensitive to external stimuli. Since the experimental discovery of CNSs,[13–15] extensive investigations have been made on their dynamical,[16] structural,[16–20] electronic, and optical[20–22] properties with molecular dynamics (MD) simulations. Although CNSs share many interesting features with CNTs, one important difference is that the core radius of a CNS is much more sensitive to the surface energy, the interlayer spacing, the bending stiffness, and the length of the associated graphene sheet.[23]

[*] Prof. H. Gao, X. Shi
Division of Engineering, Brown University
610 Barus & Holley, 182 Hope Street
Providence, RI 02912 (USA)
E-mail: Huajian_Gao@brown.edu
Y. Cheng
Institute of High Performance Computing
Singapore 138632 (Singapore)
N. M. Pugno
Department of Structural Engineering, Politecnico di Torino
Corso Duca degli Abruzzi 24, 10129, Torino (Italy)

Supporting Information is available on the WWW under http://www.small-journal.com or from the author.

DOI: 10.1002/smll.200902286

2. Methods

In the proposed CNS-based water channel, the forming graphene is taken to be semiconducting with prescribed length, bending stiffness, and interlayer spacing. Attention is focused on the effect of the core radius of the resulting CNS on water transport and how its core size depends on the effective surface energy, which can be controlled by an applied electric field. The electric field will cause the carbon atoms to be polarized with the following dipole–dipole interactions[24]

$$V\left(\vec{r}_{ij}\right) = \frac{1}{4\pi\varepsilon_0\left|\vec{r}_{ij}\right|^3}\left[\left|\vec{p}_i\right|\left|\vec{p}_j\right| - \frac{3\left(\vec{r}_{ij}\cdot\vec{p}_i\right)\left(\vec{r}_{ij}\cdot\vec{p}_j\right)}{\left|\vec{r}_{ij}\right|^2}\right] \quad (1)$$

where $\vec{r}_{ij}$ is the distance between dipole i and dipole j, $\vec{p}_i = 4\pi\varepsilon_0\alpha_i\vec{E}$ is the induced dipole moment, E being the applied electric field, ε_0 the vacuum permittivity, and α_i the polarizability of atom i. It has been previously shown that the polarizability of SWCNTs in the axial direction is one order of magnitude higher than that perpendicular to the axis.[25] Therefore, for simplicity, we will only consider the axial polarizability of carbon atoms in the CNS. The total

dipole–dipole interaction energy is

$$\Phi_{\text{dipole}} = \sum_{i \neq j} V\left(\vec{r}_{ij}\right) \quad (2)$$

from which the surface energy of the CNS can be extracted as[23]

$$\gamma_{\text{dipole}} = \frac{1}{2\pi L} \frac{d\Phi_{\text{dipole}}}{d(r_0 + R)} \quad (3)$$

where L is the axial length, and r_0 and R are the inner and outer radii of the CNS, respectively. More details of this calculation are described in the Supporting Information. The total effective surface energy of the CNS is thus

$$\gamma_{\text{eff}} = \gamma_{\text{vdW}} + \gamma_{\text{dipole}} \quad (4)$$

where γ_{vdW} is the surface energy due to van der Waals interactions between carbon atoms. Figure 1A shows that the total dipole interaction energy is indeed linearly proportional to the sum of the inner and outer radii of the CNS, with a negative slope proportional to γ_{dipole}, in perfect consistency with Equation (3). The fact that γ_{dipole} is negative indicates that the applied electric field decreases the effective surface energy. Figure 1B shows how the applied electric field influences the dipole-induced surface energy γ_{dipole} normalized by γ_{vdW}, typically about 0.2 N m^{-1}.[23] The result shows that an applied electric field of $E = 0.3$ V nm^{-1} would decrease the surface energy of the CNS by about 11.5% for graphene length $B = 50$ nm and by 36% for $B = 500$ nm. As the electric field E varies in the range from 0 to 0.5 V nm^{-1}, the normalized dipole surface energy changes from 0% to 32.7% for $B = 50$ nm and from 0% to 100% for $B = 500$ nm, indicating that the electric field can significantly alter the surface energy. This is somewhat similar to the effect of dipole–dipole interaction on the surface energy of a thin film.[26]

In our simulations, a graphene sheet of dimension 20×4 nm^2 is rolled into a zigzag CNS with axial length equal to 4 nm (Figure 2B and C). The CNS is then embedded in a lipid bilayer consisting of 128 dipalmitoylphosphatidylcholine (DPPC) molecules that are downloaded from Reference [27] (Figure 2A). The head group of DPPC molecules is constrained along the axial direction of CNS with a force constant 1000 kJ mol^{-1} nm^{-1} to ensure a stable simulation system. Tip3p water molecules[28] are added until the membrane patch is fully hydrated at 50 water molecules per lipid. The simulation package Gromacs4[29] is then used to simulate the structure and transport of water inside the CNS. The electrostatic interaction of water solvent is evaluated by the particle mesh Ewald method (PME).[30,31] A cut-off distance of 1.4 nm is used for both Ewald and van der Waals interactions. A room temperature of 300 K and an atmospheric pressure of 1 bar are maintained by the v-rescale method[32] and the Parrinello–Rahman method,[33] respectively, both at a time increment of 0.1 ps. Periodic boundary conditions and a simulation time step of 2 fs are adopted in all simulations. The system is first equilibrated for 2 ns, then followed by a 10 ns run to determine the flow rate of water. The carbon–carbon bond length 0.142 nm and angle 120° are maintained by a Morse bond, a harmonic cosine of the bending angle, and a twofold torsion potential.[34] The nonbonded van der Waals interactions are described by the Lennard–Jones (LJ) potential with parameters listed in Table 1. In our simulations, an external electric field is applied along the axial direction of CNS and directly influences the behaviors of water and lipid molecules. On the other hand, the carbon atoms in the CNS are modeled as nonpolar, except that the core size of the CNS changes in response to the electric field. According to Figure 1, the effect of an

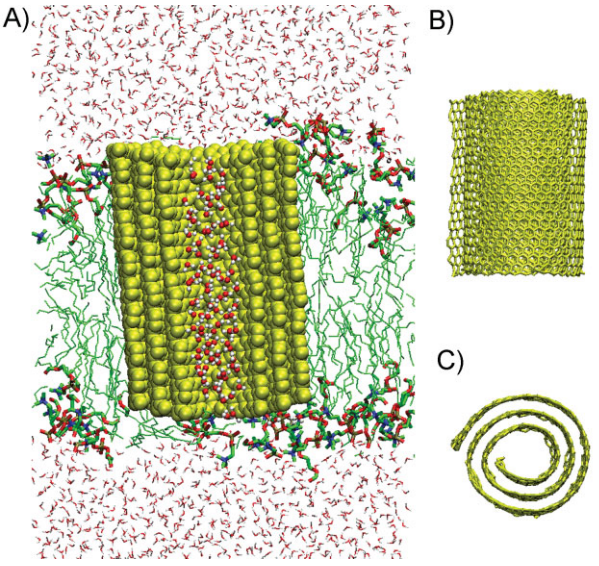

Figure 2. The CNS-based water channel. A) The water box with the CNS serving as a water channel embedded inside a DPPC bilayer. B) Side and C) top views of the CNS.

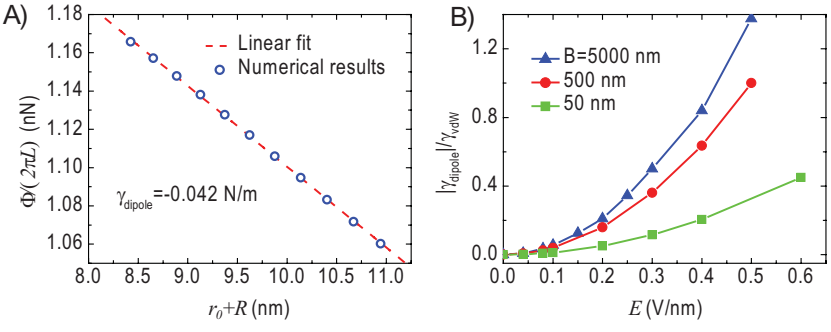

Figure 1. A) Dipole–dipole interaction energy of a CNS as a function of the sum of the inner and outer radii. The slope provides an estimate of the dipole-induced surface energy of the CNS to be about −0.042 nN nm^{-1} with an electric field of $E = 0.1$ V nm^{-1}. B) Dipole-induced surface energy (normalized by van der Waals interaction energy) as a function of the applied electric field for different lengths of graphene.

NANO MICRO small

Table 1. Interaction potential parameters.[4,34]

Interaction	ε [kJ mol^{-1}]	σ [nm]
OO	0.6367	0.3151
CC	0.3601	0.34
CO	0.4787	0.3275

applied electric field on CNSs can be represented by an effective surface energy γ_{eff}. In actual simulations, this is accomplished by multiplying the parameter ε_{CC} by a tuning factor λ so that the effective nonbonded carbon–carbon interaction is given by

$$U(r_{ij},\lambda) = 4\lambda\varepsilon_{CC}\left[\left(\frac{\sigma_{CC}}{r_{ij}}\right)^{12} - \left(\frac{\sigma_{CC}}{r_{ij}}\right)^{6}\right] \quad (5)$$

Table 2 lists all the values used in the simulations. Although the applied electric field tends to reduce the effective surface energy, that is, $\lambda < 1$, we have also considered the case of $\lambda > 1$.

3. Results

During the simulations, the CNS–water interaction energy decreases quickly for the first 0.4 ns simulations (Figure 3A). Thereafter the interaction energy is seen to gradually saturate, indicating the approach of equilibrium. Figure 4 shows that the equilibrium water structure inside the core of CNSs depends on the effective surface energy. Reducing the surface energy tends to enlarge the core size, thereby incorporating more water molecules, while increasing the surface energy tends to reduce the core size. For example, substantially more water molecules are filled inside the core in case A ($\lambda = 0.4$) than in case G ($\lambda = 1.0$). As λ is increased to 1.2, the core size becomes so small that the confined water molecules form two linear chains (Figures 4 and 5). Further increasing λ to 1.6 results in complete depletion of water from the CNS core. It can be seen in Figure 3A that the equilibrium CNS–water interaction energy decreases as more water molecules are incorporated into the core. Figure 3B shows that the number of water molecules inside the CNS, N_{water}, scales with the inverse square of the effective surface energy, that is, $N_{\text{water}} \propto 1/\gamma^2$, which can be explained from the relations $N_{\text{water}} \approx \pi r^2$ and $r \approx 1/\gamma$.[23]

It is also interesting that water molecules inside the CNS core form a spiral structure in extension of the CNS structure (Figure 4). This phenomenon is similar to previous findings that the structure of encapsulated water molecules in CNTs tends to mimic that of the confining tubular structure of graphene.[35] Figure 5 plots the radial pair distribution function of oxygen–oxygen atoms. The first peak at $r = 0.28$ nm is due to the strong hydrogen-bonding network of water. For case H ($\lambda = 1.2$), a second peak appears at $r = 0.55$ nm, corresponding to the diagonal distance of a rhombus structure formed by the two linear chains of water confined inside the core.

The flow rate of water is defined as the number of water molecules entering per unit time at one end of the CNS and leaving at the other end. Our simulations (Figure 6A) indicate that the average flow rate increases monotonically with increasing inner radius (Figure 6C). For the inner radius of 0.35 nm, the flow rate is about 30 ns^{-1}, which is comparable to Hummer's results for water flow inside a (6,6) CNT.[4] As the inner radius is increased to 0.95 nm, the flow rate increases to 284 ns^{-1}. Considering the fact that there is no osmotic pressure in our system, the change in flow rate can be attributed to changes in core size and water diffusivity in the axial direction D_{axial}. To determine D_{axial}, we first calculate the axial diffusivity of each water molecule that are or were once inside the CNS, and then perform a weighted average of the calculated values with respect to the corresponding probability distribution function shown in Figure 6B. Figure 6D displays the calculated diffusivity as a function of the core radius. In the absence of an electric field, the CNS–water interaction energy would decrease as the core size is increased, resulting in increasing water diffusivity. For example, the CNS–water interaction energy is about -17 kJ mol^{-1} when $r = 0.35$ nm ($\lambda = 1.2$) and -9.4 kJ mol^{-1} when $r = 0.48$ nm ($\lambda = 1.0$). These behaviors are consistent with previous findings that the diffusivity of water inside a CNT increases with the CNT radius.[36] However, this trend is seen to be completely reversed by the presence of an applied electric field. Figure 6D shows that as an electric field is applied to expand the core of CNS, water diffusivity decreases rather than increases as expected from the size effect alone. This phenomenon can be attributed to enhanced alignment of water dipoles along the direction of the electric field, which tends to decrease the diffusivity. A similar phenomenon has also been reported in the study of water flow through CNTs in the presence of an electric field.[7]

To investigate the effect of an applied AC electric field, in which case the effective surface energy changes with time, we consider

$$\lambda(t) = \frac{1-\beta}{2}[1 + \cos(2\pi f t)] + \beta \quad (6)$$

where f is the frequency of the AC field and β is a parameter depending on the field strength. Here we set $\beta = 0.4$ so that λ varies from 0.4 to 1 (Figure 7A). Simulations are conducted with the frequency f set at 0.25 and 0.125 GHz. The results show that the inner radius of the CNS varies periodically with

Table 2. Tuning parameter λ for different carbon–carbon interactions and the corresponding effective surface energies and electric fields.

	A	B	C	D	E	F	G	H	I
λ	0.4	0.5	0.6	0.7	0.8	0.9	1.0	1.2	1.6
r [nm]	0.99	0.95	0.81	0.72	0.67	0.61	0.48	0.35	0.18
γ_{eff} [nN nm^{-1}]	0.122	0.134	0.141	0.163	0.181	0.196	0.212	0.354	0.789
E [V nm^{-1}]	0.39	0.36	0.34	0.29	0.23	0.16	0	–	–

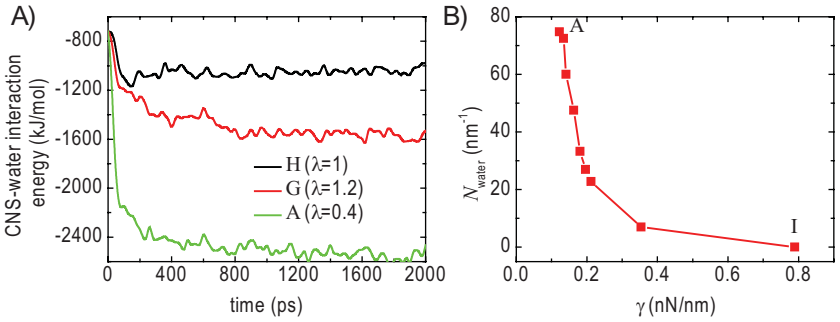

Figure 3. A) The simulated evolution of CNS–water interaction energy as a function of the simulation time. The interaction energy decreases quickly for the first 400 ps and gradually reaches an equilibrium value. B) The number of water molecules per unit axial length confined inside the CNS as a function of the effective surface energy. The parameters listed in Tables 1 and 2 are adopted.

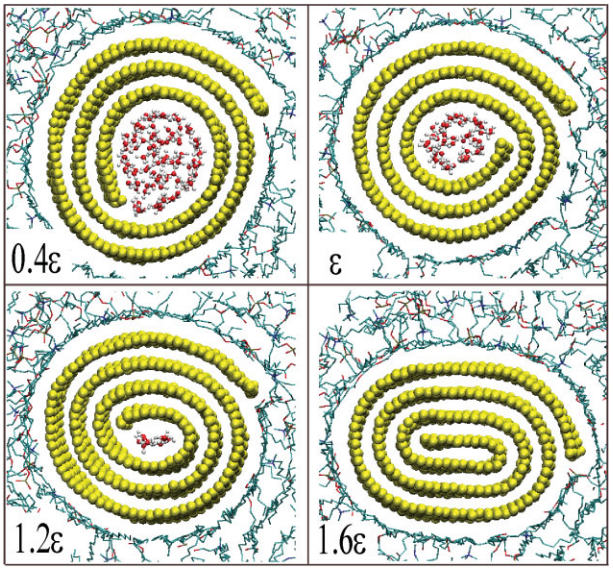

Figure 4. Simulation snapshots of CNSs with water molecules confined inside the inner core for different values of the effective surface energy. Water molecules outside the inner core are not shown for clarity.

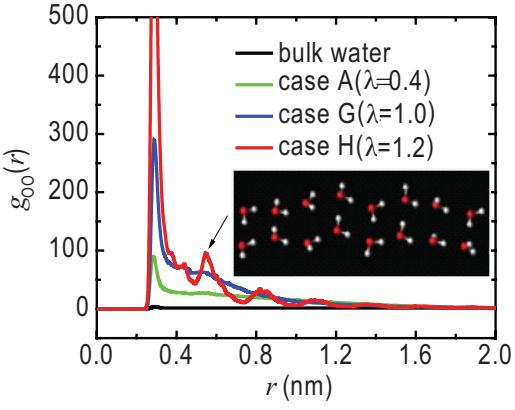

Figure 5. Radial distribution functions (RDF) of oxygen atoms in four different cases. Inset: the configuration of two linear chains of confined water molecules in case H ($\lambda = 1.2$).

the same frequency as that of the applied AC field. The variation of the number of water molecules inside the CNS is shown in Figure 7B. The maximum number of confined water molecules (about 100 nm^{-1}) is much larger than that in the DC case of $\lambda = 0.4$ (about 75 nm^{-1}), indicating that the core of the CNS can be expanded to a much larger size under an AC field. It is also found that the AC flow rates are greatly enhanced in comparison with the corresponding results under a DC field, as shown in Table 3. When $f = 0.125$ GHz and λ varies from 0.4 to 1, the mean flow rate is about 386 ns^{-1}, which can be compared to the DC flow rate of 305 ns^{-1} when $\lambda = 0.4$. When $f = 0.25$ GHz, the mean flow rate is further enhanced to 589 ns^{-1}, nearly twice the corresponding value in the DC case of $\lambda = 0.4$. This increase in mean flow rate at increasing frequency f, combined with the fact that the AC flow rates are significantly higher than the DC flow rates, may indicate a resonance phenomenon, although much further work is required to clarify the detailed mechanism. It seems that the enhanced AC flow rate can be attributed to pulsated flow stimulated by periodic contraction of the CNS. Table 3 also shows that the mean axial diffusivities of water molecules under an AC field are larger than the corresponding upper bound in the DC case of $\lambda = 0.4$ ($D_{axial} = 3.37 \times 10^{-5}$ cm^2 s^{-1}). Therefore, it seems that an AC electric field can greatly stimulate and enhance water flow in CNSs.

4. Conclusions

In summary, we have conducted MD simulations of a novel class of tunable water channels based on CNSs. We have shown that it is possible to use dipole–dipole interactions induced by an externally applied electric field to reduce the effective surface energy of a CNS, so as to controllably increase its core size and the associated water flow rate. We further showed that an applied AC field can greatly enhance the flow rates in comparison with a DC field. Compared with CNT-based water channels, the CNS-based channels exhibit much greater water permeability and sensitivity to an applied DC/AC electric field. Besides possible applications as water channels, our tunable CNS channel model can also serve as ion channels across cellular membrane or controllable nanofilters. The tunable core size can effectively prevent the passing of heavy metal ions or nanoparticles.

We also point out some potential pitfalls of our study. Figure 1B shows that the surface energy of a CNS will be significantly altered only by an applied electric field on the order of 0.2 V nm^{-1}. This value is quite high compared to the typical membrane potential of ≈0.016–0.027 V nm^{-1}[7]). The electric field used in our simulations is in the range of 0–0.39 V nm^{-1}, while the breakdown strength of membrane has been reported to be around 0.14 V nm^{-1}.[37] Although Figure 1B shows that it

NANO MICRO small

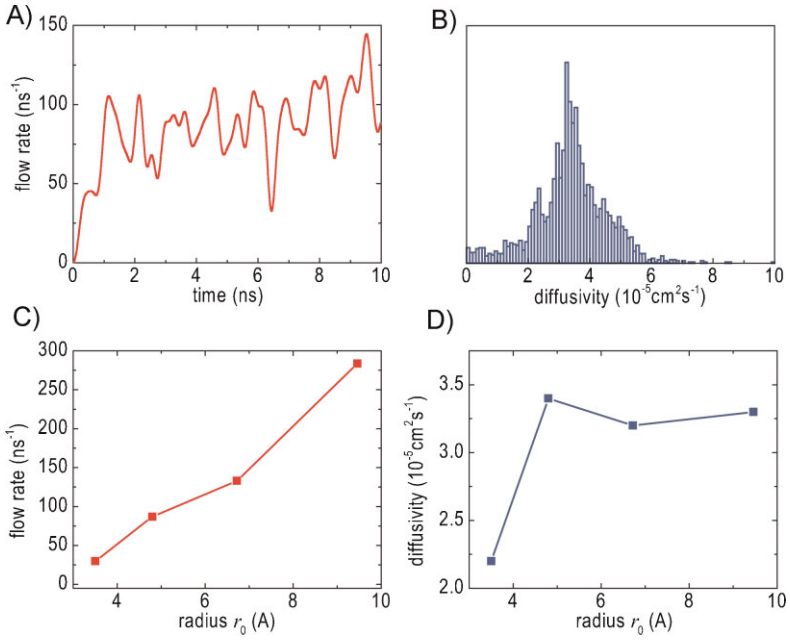

Figure 6. Flow rate and diffusivity of water in the CNS. A) Flow rate as a function of time for case G ($\lambda = 1.0$). The data has been smoothed with a fast Fourier transform (FFT) filter with 0.3 ns width. B) Probability distribution of axial diffusivity of water confined inside the CNS for case G ($\lambda = 1.0$). C) Averaged flow rate as a function of the core size of the CNS. D) Averaged water axial diffusivity as a function of the core size of the CNS. The four points represent $\lambda = 0.5$, 0.8, 1.0, and 1.2, in decreasing order of r_0.

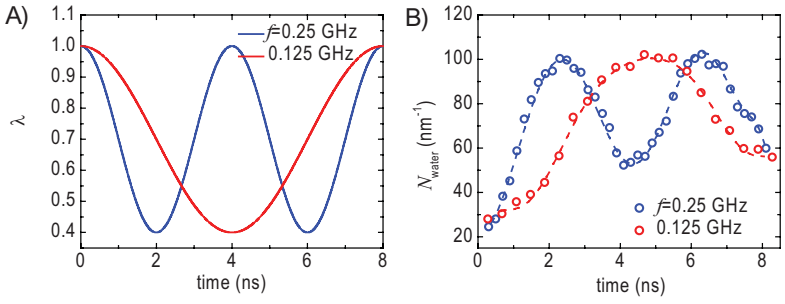

Figure 7. A) Tuning parameter λ as a function of time. B) The number of water molecules per unit axial length confined inside the CNS as a function of time.

is certainly possible to achieve full tuning of CNSs within the breakdown strength of membrane by increasing the length of the basal graphene sheet, it will be important from a practical point of view to investigate strategies to enhance the sensitivity of CNSs to an applied electric field through functionalization and/or to tune the surface energy of CNSs via other applied fields. Further studies will be directed along this line of research in the future.

Table 3. Tuning parameter λ and f for different carbon–carbon interactions and the corresponding water flow rates and axial diffusivities within the CNS core.

	Flow rate [ns^{-1}]	Axial diffusivity [10^{-5} cm^2 s^{-1}]
DC: $\lambda = 0.4$	305	3.37
AC: $\lambda \approx 0.4$–1, $f = 0.125$ GHz	386	3.42
AC: $\lambda \approx 0.4$–1, $f = 0.25$ GHz	589	3.58

[1] A. S. Verkman, A. N. VanHoek, T. H. Ma, A. Frigeri, W. R. Skach, A. Mitra, B. K. Tamarappoo, J. Frainas, *Am. J. Physiol.: Cell Physiol.* **1996**, *270*, C12–C30.
[2] M. A. Knepper, *Am. J. Physiol. Renal* **1997**, *272*, F3–F12.
[3] E. Steudle, T. Henzler, *J. Exp. Bot.* **1995**, *46*, 1067–1076.
[4] G. Hummer, J. C. Rasaiah, J. P. Noworyta, *Nature* **2001**, *414*, 188–190.
[5] R. Z. Wan, J. Y. Li, H. J. Lu, H. P. Fang, *J. Am. Chem. Soc.* **2005**, *127*, 7166–7170.
[6] S. Joseph, N. R. Aluru, *Phys. Rev. Lett.* **2008**, *101*, 064502.
[7] J. A. Garate, N. J. English, J. M. D. MacElroy, *Mol. Simul.* **2009**, *35*, 3–12.
[8] F. Q. Zhu, K. Schulten, *Biophys. J.* **2003**, *85*, 236–244.
[9] B. Liu, X. Li, B. Li, B. Xu, Y. Zhao, *Nano Lett.* **2009**, *9*, 1386–1394.
[10] S. Joseph, R. J. Mashl, E. Jakobsson, N. R. Aluru, *Nano Lett.* **2003**, *3*, 1399–1403.
[11] J. Y. Li, X. J. Gong, H. J. Lu, D. Li, H. P. Fang, R. H. Zhou, *Proc. Natl. Acad. Sci. U. S. A.* **2007**, *104*, 3687–3692.
[12] X. J. Gong, J. Y. Li, H. J. Lu, R. Z. Wan, J. C. Li, J. Hu, H. P. Fang, *Nat. Nanotechnol.* **2007**, *2*, 709–712.
[13] H. Shioyama, T. Akita, *Carbon* **2003**, *41*, 179–181.
[14] L. M. Viculis, J. J. Mack, R. B. Kaner, *Science* **2003**, *299*, 1361.
[15] M. V. Savoskin, V. N. Mochalin, A. P. Yaroshenko, N. I. Lazareva, T. E. Konstantinova, I. V. Barsukov, I. G. Prokofiev, *Carbon* **2007**, *45*, 2797–2800.
[16] S. F. Braga, V. R. Coluci, S. B. Legoas, G. Giro, D. S. Galvão, R. H. Baughman, *Nano Lett.* **2004**, *4*, 881–884.
[17] S. F. Braga, V. R. Coluci, R. H. Baughman, D. S. Galvão, *Chem. Phys. Lett.* **2007**, *441*, 78–82.
[18] V. R. Coluci, S. F. Braga, R. H. Baughman, D. S. Galvão, *Phys. Rev. B* **2007**, *75*, 125404.
[19] G. Mpourmpakis, E. Tylianakis, G. E. Froudakis, *Nano Lett.* **2007**, *7*, 1893–1987.
[20] Y. Chen, J. Lu, Z. Gao, *J. Phys. Chem. C* **2007**, *111*, 1625–1630.
[21] H. Pan, Y. Feng, J. Lin, *Phys. Rev. B* **2005**, *72*, 085415.
[22] R. Rurali, V. R. Coluci, D. S. Galvão, *Phys. Rev. B* **2006**, *74*, 085414.
[23] X. H. Shi, N. M. Pugno, H. J. Gao, *J. Comput. Theor. Nanosci*, DOI: 10.1166/jctn.2010.1387.
[24] J. Israelachvili, *Intermolecular & Surface Forces*, Academic Press, London **1991**.
[25] R. Langlet, M. Devel, P. h. Lambin, *Carbon* **2006**, *44*, 2883–2895.
[26] R. Maheshwari, R. Parthasarathi, A. Dhathathreyan, *J. Colloid Interface Sci.* **2004**, *271*, 419–425.
[27] D. P. Tieleman, H. J. C. Berendsen, *J. Chem. Phys.* **1996**, *105*, 4871–4880.
[28] W. L. Jorgensen, J. Chandrasekhar, J. D. Madura, R. W. Impey, M. L. Klein, *J. Chem. Phys.* **1983**, *79*, 926–935.
[29] B. Hess, C. Kutzner, D. van der Spoel, E. Lindahl, *J. Chem. Theory Comput.* **2008**, *4*, 435447.

[30] T. Darden, D. York, L. Pedersen, *J. Chem. Phys.* **1993**, *98*, 10089–10092.
[31] U. Essmann, L. Perera, M. L. Berkowitz, T. Darden, H. Lee, L. G. Pedersen, *J. Chem. Phys.* **1995**, *103*, 8577–8593.
[32] G. Bussi, D. Donadio, M. Parrinello, *J. Chem. Phys.* **2007**, *126*, 014101.
[33] M. Parrinello, A. Rahman, *J. Appl. Phys.* **1981**, *52*, 7182–7190.
[34] J. H. Walther, R. Jaffe, T. Halicioglu, P. Koumoutsakos, *J. Phys. Chem. B* **2001**, *105*, 9980–9987.
[35] J. Zou, B. Ji, X. Feng, H. Gao, *Small*, **2006**, *2*, 1348–1355.
[36] Y. C. Liu, J. W. Shen, K. E. Gubbins, J. D. Moore, T. Wu, Q. Wang, *Phys. Rev. B* **2008**, *77*, 125438.
[37] D. P. Tieleman, H. Leontiadou, A. E. Mark, S. J. Marrink, *J. Am. Chem. Soc.* **2003**, *125*, 6382–6383.

Received: December 8, 2009
Published online: March 1, 2010

Supplementary

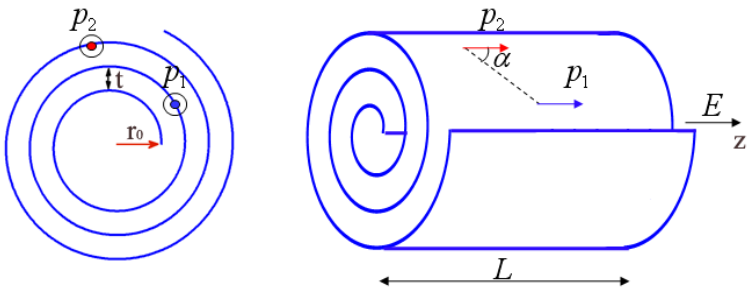

Dipole-dipole interaction energy

For arbitrary two dipoles induced by electric field E with dipole moment P_1 and P_2, the interaction energy is

$$V(\vec{r}_{12}) = \frac{1}{4\pi\varepsilon_0 |\vec{r}_{12}|^3}\left[|\vec{p}_1||\vec{p}_2| - \frac{3(\vec{r}_{12}\cdot\vec{p}_1)(\vec{r}_{12}\cdot\vec{p}_2)}{|\vec{r}_{12}|^2}\right], \tag{S1}$$

where

$$|\vec{r}_{12}| = \sqrt{\tilde{r}_1^2 + \tilde{r}_2^2 - 2\tilde{r}_1\tilde{r}_2\cos(\theta_1-\theta_2)+z^2}\,, \tag{S2}$$

is the distance of the two dipoles and

$$\begin{aligned}\tilde{r}_1 &= r_0 + \frac{t}{2\pi}\theta_1,\\ \tilde{r}_2 &= r_0 + \frac{t}{2\pi}\theta_2.\end{aligned} \tag{S3}$$

Suppose each carbon atoms in the CNS is polarized in the electric field, then the total dipole-dipole interaction is

$$\Phi_{dipole} = \sum_{i\neq j} V(\vec{r}_{ij}), \tag{S4}$$

which can be calculated as

$$\Phi_{dipole} = \rho_1\rho_2 \int_0^L dz' \int_0^{2\pi N} \tilde{r}_1 d\theta_1 \int_{\theta_1}^{2\pi N} \tilde{r}_2 d\theta_2 \int_{-z'}^{L-z'} \frac{1}{4\pi\varepsilon_0 \left|\vec{r}_{12}^{\,3}\right|} \left[p_1 p_2 - 3p_1 p_2 \cos^2\alpha\right] dz, \qquad \text{(S5)}$$

where ρ_1, ρ_2 are the dipole densities, N is the winding number of the CNS, $\cos\alpha = \frac{z}{|\vec{r}_{12}|}$.

Integrate Eq. (S5) we obtain

$$\Phi_{dipole} = \frac{(4\pi\varepsilon_0 E)^2 \rho_1\rho_2}{2\pi\varepsilon_0} e_{dipole}(N, L, r_0, t), \qquad \text{(S6)}$$

where

$$e_{dipole}(N, L, r_0, t) = \int_0^{2\pi N} \int_{\theta_1}^{2\pi N} \tilde{r}_1\tilde{r}_2\alpha_1\alpha_2 \left(\frac{1}{\sqrt{\tilde{r}_1^2 + \tilde{r}_2^2 - 2\tilde{r}_1\tilde{r}_2\cos(\theta_1 - \theta_2)}} - \frac{1}{\sqrt{\tilde{r}_1^2 + \tilde{r}_2^2 + L^2 - 2\tilde{r}_1\tilde{r}_2\cos(\theta_1 - \theta_2)}} \right) d\theta_2 d\theta_1. \qquad \text{(S7)}$$

For the axial polarizability α_i, Langlet *et. al.* have found the relationship between α_i and CNTs radius r as

$$\alpha_i = (50.1348r + 10.8091). \qquad \text{(S8)}$$

Since the value of α_i obtained in Reference S1 is polarizability per unit length of CNTs, we transform it to polarizability per atom in our case by

$$\alpha_i = (50.1348\tilde{r}_i + 10.8091)\frac{\sqrt{3}a}{2\pi\tilde{r}_i} 0.5a, \qquad \text{(S9)}$$

where a is the carbon-carbon bond length. It is worth pointing out that in Reference S1 the authors have considered the local electric field effect, *i.e.* the electric field induced by dipole, so by adopting the results, we have indeed included the dipole screening effect into our model.

Reference

(S1) R. Langlet, M. Devel, Ph. Lambin, *Carbon*, **2006**, *44*, 2883-2895.